Journal of Materials Chemistry A

RSC Publishing

COMMUNICATION

View Article Online
View Journal | View Issue

Grafting density effects, optoelectrical properties and nano-patterning of poly(*para*-phenylene) brushes†

Cite this: *J. Mater. Chem. A*, 2013, **1**, 13426

Received 15th July 2013
Accepted 17th September 2013

DOI: 10.1039/c3ta12745a

www.rsc.org/MaterialsA

Jihua Chen,*[a] Jose Alonzo,[a] Xiang Yu,[b] Kunlun Hong,[a] Jamie M. Messman,[a] Ilia Ivanov,[a] Nickolay V. Lavrik,[a] Moloy Banerjee,[c] Rajendra Rathore,[c] Zhenzhong Sun,[d] Dawen Li,[d] Jimmy W. Mays,[be] Bobby G. Sumpter[af] and S. Michael Kilbey II*[eg]

Well-defined conjugated polymers in confined geometries are challenging to synthesize and characterize, yet they are potentially useful in a broad range of organic optoelectronic devices such as transistors, light emitting diodes, solar cells, sensors, and nanocircuits. Herein we report a systematic study of optoelectrical properties, grafting density effects, and nanopatterning of a model, end-tethered conjugated polymer system. Specifically, poly(*para*-phenylene) (PPP) brushes of various grafting density are created *in situ* by aromatizing well-defined, end-tethered poly(1,3-cyclohexadiene) (PCHD) "precursor brushes". This novel precursor brush approach provides a convenient way to make and systematically control the grafting density of high molecular weight conjugated polymer brushes that would otherwise be insoluble. This allows us to examine how grafting density impacts the effective conjugation length of the conjugated PPP brushes and to adapt the fabrication method to develop spatially patterned conjugated brush systems, which is important for practical applications of conjugated polymer brushes.

Polymer brushes, which are created by tethering chains by one of their ends to a surface or interface, are model systems for studying structure–property relationships of confined thin films and may serve as a basis to understand polymer micelles, polymer-stabilized colloid particles, or interfaces compatibilized by block or graft copolymers.[1,2] Brushes are also model systems for studying fundamental behavior such as adhesion, friction, and anti-fouling characteristics, and the preferentially *stretched, upright configuration* of the chains caused by tethering serves as a useful "handle" for tailoring the range and strength of interactions across interfaces. For analogous reasons, layers of end-grafted conjugated polymers preferentially oriented at interfaces are potentially important for a variety of organic optoelectronic applications.[3–6] Conjugated polymer brushes remain in a nascent state of development, due in part to challenges in growing conjugated polymers from surfaces[7–9] or to limitations in the grafting density achieved when attaching end-functionalized conjugated polymers to a surface.[10] Despite these challenges, several groups have recently reported[7–9] the use of catalyst-transfer surface-initiated polycondensation to grow conjugated polymer brushes, including poly(*para*-alkoxyphenylene), polyfluorene, and poly(3-alkylthiophene). However, surface initiated polymerizations have several limitations: (1) it is difficult to assess polymer characteristics such as molecular weight and polydispersity; (2) the molecular weight of the polymer chains may often be limited by solubility or the entropic penalty for stretching; and (3) the process requires a non-trivial step of initiator immobilization as well as a complicated experimental setup.[7–9] Using "click" chemistry to graft pre-made chains to a surface can address some of those issues[10] but it is restricted to systems with satisfactory solubility. In addition, because of the barrier posed by the growing, crowded layer, achieving a wide variation in grafting density can be difficult.

In this work, we advance the use of post-attachment conversion of a neutral, precursor brush to create conjugated poly(*para*-phenylene) (PPP) brushes. The approach allows grafting density of chains to be systematically altered, allowing its role on effective conjugation length to be examined. PPP is well-known for its high thermal and chemical stability, as well its highly desirable optoelectrical properties.[11–17] Recently, we

[a]*Center for Nanophase Materials Sciences, Oak Ridge National Laboratory, Oak Ridge, TN 37831, USA. E-mail: chenj1@ornl.gov*

[b]*Chemical Sciences Division, Oak Ridge National Laboratory, Oak Ridge, TN 37831, USA*

[c]*Department of Chemistry, Marquette University, Milwaukee, WI 53201, USA*

[d]*Department of Electrical and Computer Engineering, University of Alabama, Tuscaloosa, AL 35487, USA*

[e]*Department of Chemistry, University of Tennessee, Knoxville, TN 37996, USA. E-mail: mkilbey@utk.edu*

[f]*Computer Science and Mathematics Division, Oak Ridge National Laboratory, Oak Ridge, TN 37831, USA*

[g]*Department of Chemical and Biomolecular Engineering, University of Tennessee, Knoxville, TN 37996, USA*

† Electronic supplementary information (ESI) available: Experimental details, extracted λ_{max} *vs.* $1/n$ plot, impedance spectroscopy of PCHD and PPP brush on heavily doped silicon wafer, and doping mechanism of PPP brush in $FeCl_3/CH_3NO_2$ solution. See DOI: 10.1039/c3ta12745a

reported a "precursor brush" method to create PPP brushes from trichlorosilane end-functionalized poly(1,3-cyclohexadiene) (PCHD) chains of different molecular weights (M_n = 4k–19k) synthesized by anionic polymerization.[18] This approach allows the chain properties of the precursor PCHDs to be fully characterized, successfully circumvents the limited solubility and poor processibility of PPP, and allows layers of high molecular weight PPPs to be created and studied.[18] PPP brushes fabricated with the precursor method are a useful model system for studying conjugated polymer brushes because of the low-polydispersity (PDI < 1.1), high molecular weight (M_n = 4k–19k), and the predominant 1,4 stereoregularity (~95%) that is difficult to achieve otherwise. While our previous work was mainly focused on synthesis, demonstrating brush formation, and molecular characterization of PPP brushes, this current work addresses the effect of grafting density, doping, micro- and nano-patterning of the PPP brushes. Because it regulates the extent of stretching due to interchain interactions, grafting density is an important parameter in polymer brush systems. Here the ability to manipulate grafting density through the use of soluble precursor polymers provides an opportunity to systematically examine the effect of grafting density on electronic properties, such as the effective conjugation length. Similarly, while efforts to dope and pattern conjugated polymers are routine, reports describing doping and patterning of conjugated polymer brushes are rare, despite the fact that such systems may be useful for applications for optoelectronic devices.[19]

Fig. 1a shows the scheme by which PPP brushes are created by *in situ* aromatization of PCHD brushes.[18] Trichlorosilane end-functionalized PCHDs are deposited by spin-coating from dilute solution onto "piranha acid" or UV-ozone cleaned substrates (silicon wafers or quartz, respectively), and the resultant films are thermally annealed at 160 °C under vacuum. Subsequently, the surface-attached PCHD brushes are immersed for 2 days in 350 mL 1,2-dichlorobenzene (ODCB) with 1.4 g L^{-1} 2,3-dichloro-5,6-dicyanobenzoquinone (DDQ) at 120 °C to yield PPP brushes. The resultant PPP brushes are rinsed successively with copious amounts of acetone, toluene, and benzene, and then subjected to ultrasonication in benzene for 1 hour before drying with a stream of dry nitrogen. The molecular weight, thickness and graft density of the final PPP brushes are determined based on the PCHD precursors and spin-coating conditions, which is a clear advantage of this novel method for fabricating conjugated polymer brushes. Since our previous study[18] compared the morphology of a PCHD brush and its converted PPP analog at a single molecular weight and film thickness, here we elaborate on the morphological changes by examining brushes as a function of molecular weight, film thickness, and grafting density (Fig. 1b–d). Fig. 1b shows the effect of molecular weight on the surface morphology of PPP brushes created to have a constant thickness (nominally about 15 nm for all of the molecular weights) and Fig. 1c shows the surface morphology of PPP brushes created with the PCHD having the lowest number-average molecular weight ($M_{n,PCHD}$ = 4k) as a function of film thickness (9 nm, 15 nm and 34 nm, as measured by ellipsometry). Consistent with our earlier report,[18] we observe that the film topology changes upon transformation from PCHD to PPP, with the topology of the PPP brushes being more grainy and rougher than their PCHD counterparts. The grain size information extracted from AFM experiments and thickness measurements is summarized in Fig. 1e. Grain sizes of the PPP brushes are found, in general, to increase as the film thickness increases, regardless of the molecular weight of the precursor PCHD brush; this is, likely caused by interchain π–π interactions, which drive chain aggregation, leading to distinctive domains that are absent in their non-conjugated counterparts, the PCHD precursor brushes. The grafting density σ of a PPP (or PCHD) brush, calculated from the dimensional expression $\sigma = t\rho N_{Av}/M_n$, where t is the brush film thickness, ρ is the polymer density, N_{Av} is Avogadro's number, and M_n is the number-average molecular weight of the polymer, is plotted as a function of film thickness in Fig. 1d. The thicknesses of the PCHD and PPP brushes are obtained from ellipsometry measurements.[18] The repeat unit molecule weights of the PCHD and its corresponding PPP brush are 80 and 76 g mol^{-1}, so upon aromatization the M_n values of polymers change only slightly, from 4.3k, 11.7k, and 19.0k for PCHD, to 4.1k, 11.1k, and 18.1k for PPP. To link the PPP brushes to their corresponding PCHD precursors, we simply designate these as PPP 4k, PPP 11k and PPP 19k throughout the rest of the manuscript. Alonzo, *et al.* previously reported that the grafting density of PCHD and PPP brushes could be varied from 0.2 to 1.5 chains per nm^2 for M_n = 11k, and from 0.3 to 0.9 chains per nm^2 for M_n = 19k.[18] In the current work, by varying spin-coating conditions used to apply the PCHD precursors, it was possible to extend the range of grafting density considerably, even for chains of higher molecular weight: grafting densities reached 7 chains per nm^2 for M_n = 4.3k and up to 4.7 chains per nm^2 for M_n = 19k. This increase in range is instrumental in locating the optimal grafting density and effective conjugation length (Fig. 2 and the related discussion). To examine whether the thicknesses achieved for the PCHD are reasonable, the contour length of the PCHD chains were calculated assuming only 1,4 linkages between monomer units and a monomer size of 0.433 nm.[20] Contour lengths of 25 nm, 68 nm, and 110 nm are obtained for PCHD chains having 54, 146 and 239 repeat units, respectively. (These correspond to the 4k, 11k, and 19k PCHDs.) While these values may suggest that the 4k and 19k chains are fully stretched, it should be cautioned that molecular weights reported are relative (to polystyrene standards) and no accounting for the breadth of the molar mass distribution is made. In addition, the change in polarization of light that is interpreted as an ellipsometric thicknesses depends sensitively on the thickness and refractive index, which are coupled in thin film systems. In consideration of these elements, the layer thicknesses reported are reasonable and probably best viewed as representing strongly stretched PCHD chains. Our prior work shows that even at grafting densities of 0.2 chains per nm^2, tethered PCHDs of these molecular weights are laterally crowded and, therefore stretch away from the grafting surface, forming brushes.[18] Moreover, grazing angle attenuated total reflectance Fourier transform infrared spectroscopy (GATR-FTIR) shows disappearance of CH_2 stretching bands between 2018 and 2858 cm^{-1}, indicating (within the sensitivity of the technique) complete conversion of the brushes from PCHD to PPP when

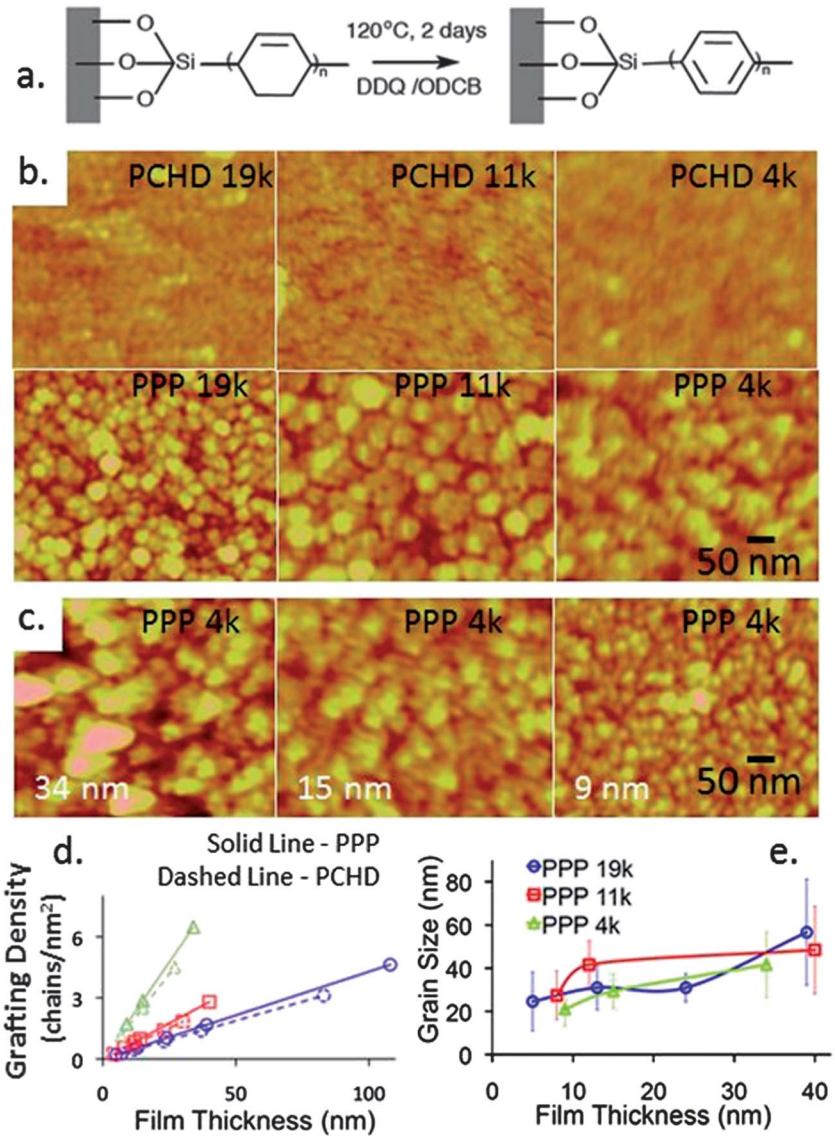

Fig. 1 Synthesis of PPP brushes and the effects of molecular weight, thickness, and grafting density on surface morphology. (a) The PPP brush was fabricated by direct aromatization of PCHD brush. (b) AFM images of PCHD brushes with different molecular weight (M_n = 4k, 11k, and 19k) and the corresponding PPP brushes. The film (brush) thickness is ~15 nm for all PCHD and PPP brushes shown here. (c) The effect of PPP brush thickness on surface morphology by AFM. The molecular weight of PPP brush shown here is 4k and the thickness values are labeled at the bottom left corner of each image. (d) The effect of thickness and molecular weight of PPP brushes (solid lines) and PCHD brushes (dashed lines) on grafting density and (e) grain sizes. For a given molecular weight, larger grafting density is generally correlated with a larger grain sizes in PPP brushes.

aromatization is conducted using DDQ at 120 °C under nitrogen for more than 36 h.[18]

UV-Vis spectra of the PPP brushes are shown as a function of molecular weight and film thickness in Fig. 2a. Spectra of the PCHD brushes are featureless, consistent with our earlier work.[18] All of the PPP brushes exhibit two absorption peaks, one at about 210 nm and a second between 300 and 400 nm that shifts with molecular weight. Following the treatment of Alonzo *et al.*,[18] the absorption maxima in the 300–400 nm range was compared to those of oligo *para*-phenylenes and used to determine the conjugation length of the PPP brushes in order to understand the effect of grafting density on optoelectronic properties (Fig. S1†). Fig. 2b shows that grafting density plays a critical role in determining the effective conjugation length of the PPP brush and, at a grafting density of ~1 chains per nm^2, the effective conjugation length reaches a maximum of 5. This behavior appears to be independent of the molecular weight of the PPP brush, and the fact that the effective conjugation length goes through a maximum is likely a result of trade-offs between packing and defects: as the grafting density increases from 0.1 to 1 chains per nm^2, the PPP chains fully cover and efficiently pack along the substrate, leading to an increase in the effective conjugation length. As the grafting density increases from 1 to 7 chains per nm^2, increasing crowding and overlap of adjacent chains during the tethering processes builds conformational defects into the chain, which reduces the effective conjugation

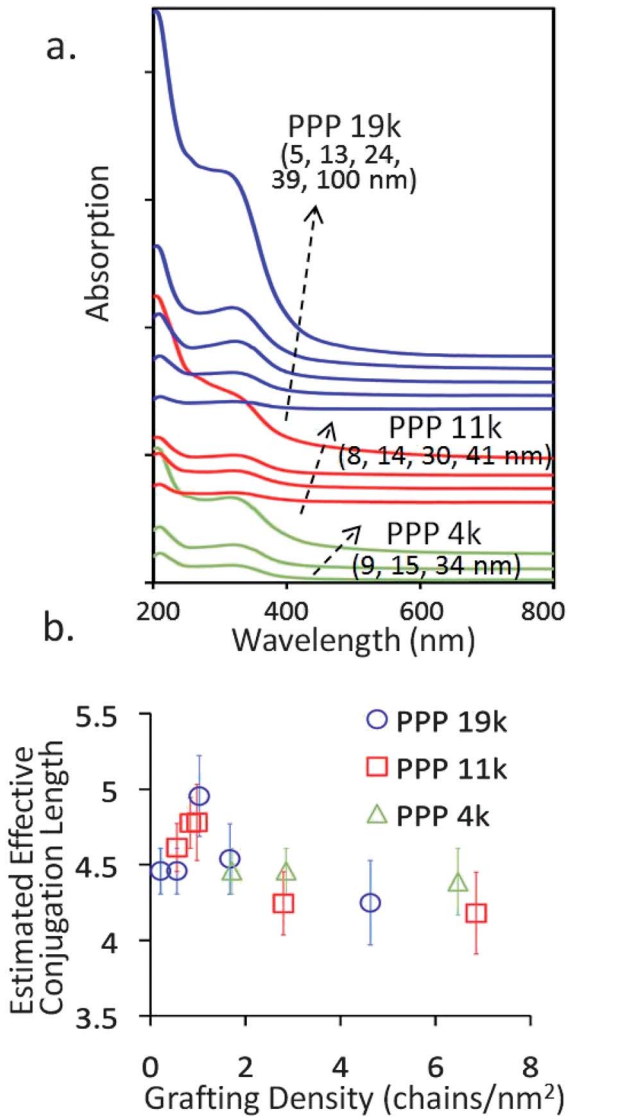

Fig. 2 The UV-Vis spectra of PPP brushes (a), and estimated conjugation length as a function of molecular weight and grafting density (b).

length. Similarly, UV-Vis spectra of poly(3-hexylthiophene) brushes showed that the vibronic shoulder that arises due to interchain processes was substantially attenuated, a behavior that was attributed to intrachain conformational defects arising because of tethering that interfered with the ability of the chains to π-stack.[19] These sets of results generally imply that there are trade-offs between the arrangement (density) of the conjugated polymer chains and their optoelectronic properties, which may be important in device applications of such systems.

Since doping and electrical properties are important aspects of fundamental understanding and practical applications of conjugated polymer and have been studied for three decades,[21–23] herein we use impedance spectroscopy to examine the electrical properties of PPP ($M_n = 4k$) brush during doping. A metal–insulator–metal configuration is used in this work (Fig. S2a†) and the PPP brush is doped by immersion in an anhydrous, saturated $FeCl_3$/nitromethane (CH_3NO_2) solution for desired lengths of time. After doping, a pattern of 0.7 mm (diameter) circular gold electrodes (50 nm thick) are deposited (at $<10^{-7}$ torr and an evaporation rate of ~1 angstrom per second) by thermal evaporation atop the polymer brushes on heavily doped silicon wafer (resistivity < 0.001 Ω cm, with 2 nm native oxide). Impedance spectra for a PCHD brush ($M_n = 4k$), as well as for undoped, lightly doped (1 day), and heavily doped PPP brushes ($M_n = 4k$, for more than 5 days) (Fig. S2b†) are obtained using an amplitude of 1 V. All of the brushes tested have a thickness of ~15 nm. Each impedance spectroscopy result (both phase and magnitude) is consistent from 5–10 individual measurements and each sample is typically cycled for 3 times in frequency domain (20 Hz to 2 MHz) with no substantial changes in behavior observed. The PCHD brushes show a large, constant phase angle that is close to 90° across the entire frequency range and the Bode plot shows a linear decrease in the magnitude of electrical impedance, which is consistent with the behavior of a simple capacitor. All of the PPP brushes show a plateau in the low frequency region of the Bode plot, with the doping process dramatically extending the range of the plateau and decreasing the magnitude of electrical impedance. The phase angles of the PPP brushes are significantly smaller than those of PCHD brushes and show a strong dependence on doping level and frequency. Equivalent circuit modeling was used to fit the real (Z') and imaginary (Z'') components of the impedance. As shown in Fig. 3, either a R(QR), where Q refers to a constant phase element (or CPE), or a Randles model (R(CR)) provides a reasonable fit of the data from the PPP brush: a Randles model gives a slightly better fit for undoped PPP brushes while the R(QR) model gives a slightly better fit in the case of the lightly doped PPP brushes. Both models fit the data acquired from the heavily doped PPP brushes equally well. The parameters extracted from equivalent circuit modeling are listed in Table 1 along with a χ^2 value, which provides a measure of the goodness-of-fit.

For both models, R_1 represents the contact resistance and R_2 corresponds to the bulk resistance (due to the PPP brush and the 2 nm native SiO_2 layer). In the R(CR) (Randles) model, C is the bulk capacitance, while in R(QR) model, $Z_{CPE} = 1/Y_o(f)^n$, where Y_o is the CPE admittance, f is frequency and n is a constant between 0 and 1. The two models are consistent in that they yield values of the PPP brush resistance (R_2) of 2–2.5 × 10^6 Ω in the undoped state, 1.6–1.8 × 10^5 Ω when lightly doped, and 2.8 × 10^3 Ω when the PPP brushes are heavily doped. Because the 2 nm thick native SiO_2 layer with no brush displays a negligible phase angle (~0 degree) and a constant resistance of 350 Ω, at frequencies lower than 100 kHz one may approximate the contribution of the native oxide layer in the circuit elements as a serially connected resistor of 350 Ω, which is significantly smaller than the extracted R_2 values reported here. Thus, while this contribution may be neglected in the current work, it does set a lower limit for the sensitivity of our measurements. Clearly, it would be difficult to measure a more highly doped PPP brush that has a resistance comparable to or lower than that of the 2 nm native oxide layer. Nevertheless, the results obtained from equivalent circuit modeling not only suggest that PPP brushes fabricated *via* the "precursor" method were

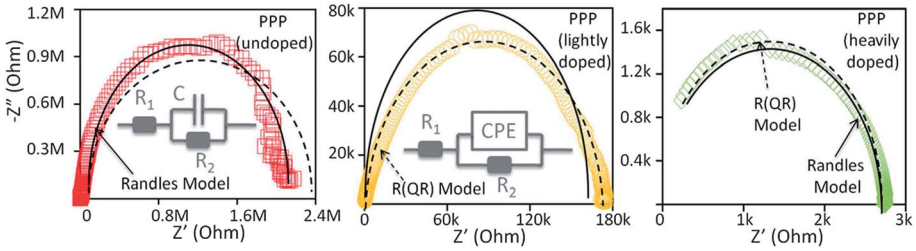

Fig. 3 Equivalent circuit modeling of an undoped PPP brush (left), a PPP brush lightly doped by exposing to the doping solution for one day (center), and a heavily doped PPP brush created by exposing to the doping solution for more than 5 days. All of these brushes were approximately 15 nm thick, created using a PCHD with M_n = 4k. Each graph shows the best fit using a Randles model (R(CR) as shown in the leftmost panel) as the solid black lines and the best fit achieved with the R(QR) model (shown in middle panel) and represented by the dashed black lines.

successfully doped, they also provide insights into the nature of the relevant interfaces (brush/substrate and brush/air). Here we assume that the interface between the brush and the silicon wafer substrate is ideally smooth in all cases. The undoped PPP brush seems to have a relatively smooth brush/electrode interface and is modeled well with a Randles model, while the impedance data of the lightly doped PPP brush are better fit by the R(QR) model, which suggest the presence of an imperfect capacitor or CPE. The need for a CPE likely originates from the increase in brush/air surface roughness during the solution doping process, accompanied with the reduction of the electrical impedance of PPP brush by 1–2 orders of magnitude within the first day of doping process. (The doping mechanism is shown in Fig. S3,† which involves a redox reaction between Fe^{2+} and Fe^{3+}.) The doping process of PPP brush is considerably slower than the reported doping of OPP powder,[25–28] which is likely caused by the confined geometry in PPP brush and the much larger molecular weights made available by our "precursor brush" method. After further doping (5 days or more), the electrical impedance of PPP brush drops by at least three orders of magnitude, and the small magnitude of electrical impedance prevents differentiation between the R(CR) and R(QR) models.

Low-cost and convenient methods of micro-patterning or nanopatterning of conjugated polymer are highly desirable.[24,29–31] Because of the chemistry involved with the precursor brush method described in this work, patterning of the resultant PPP brushes can be conveniently achieved from a metal (Ni or Cr) pattern produced by either photo- or e-beam lithography (Fig. S4†). This eliminates the requirements for more specialized and unconventional techniques such as area-selected electropolymerization, photochemical patterning, microcontact printing, or patterning of self-assembled monolayers as surface initiators.[29,32] The patterned metal template itself may be removed later with a $FeCl_3$ solution without compromising the formed brushes of conjugated polymers.[33] Thus the patterning scheme used in this work (Fig. S4†) offers a facile approach towards micro- and nano-patterning of conjugated polymer brush and, at the same time, allows systematic control of grafting density by simply varying spin-coating conditions of the precursor brush. Some representative images of micro- and nano-patterned PPP brushes are shown in Fig. 4. E-beam lithography of a PMMA film, followed by metal layer deposition and lift-off of PMMA are used to produce Ni or Cr nanodots with a 200 nm spacing (Fig. 4a), and the corresponding nano-patterned PPP brush is shown in Fig. 4b. A trace amount of metal remaining between the patterned metal nanodots resulted from the e-beam lithography and metal deposition process, and this may be responsible for some of the PPP brush boundaries seen in Fig. 4b. Similarly, a micro-patterned PPP brush is shown in Fig. 4c and 4d, which is fabricated by photolithography-generated metal micropatterns. In this case, voids from metal sacrificial layer removal are dots and the PPP brush covers the area surrounding the voids. (The peel-off of the metal sacrificial layer can be easily observed and monitored under optical microscope.)

Post-polymerization chemistry to change the nature of polymer systems is extensively practiced,[34–36] and post-polymerization

Table 1 Results of equivalent circuit modeling of PPP brushes (15 nm thickness, M_n = 4k) as a function of doping level. Standard deviation in percentage (%), enclosed in parentheses, follows each fitted parameter

		Undoped	Lightly doped (1 day)	Heavily doped (>5 days)
R(QR) model ($Z_{CPE} = 1/Y_o(jf)^n$)	R_1 (Ω)	3.7×10^{-3} (3.5×10^6)	1.8×10^{-4} (2.2×10^7)	0.010 (2.5×10^5)
	Y_o (Ω^{-1} s^n)	1.1×10^{-9} (7.5)	9.5×10^{-10} (4.3)	8.1×10^{-11} (12)
	n	0.80 (0.77)	0.81 (0.39)	1.0 (0.87)
	R_2 (Ω)	2.5×10^6 (3.4)	1.8×10^5 (0.62)	2.8×10^3 (0.98)
	χ^2	0.037	0.0031	0.0011
R(CR) model (Randles model)	R_1 (Ω)	9.0×10^3 (6.6)	6.8×10^2 (16)	1.5×10^{-5} (9.3×10^7)
	C (F)	1.3×10^{-10} (4.6)	6.6×10^{-11} (2.7)	8.1×10^{-11} (1.3)
	R_2 (Ω)	2.0×10^6 (5.9)	1.6×10^5 (2.3)	2.8×10^3 (0.53)
	χ^2	0.20	0.060	0.0012

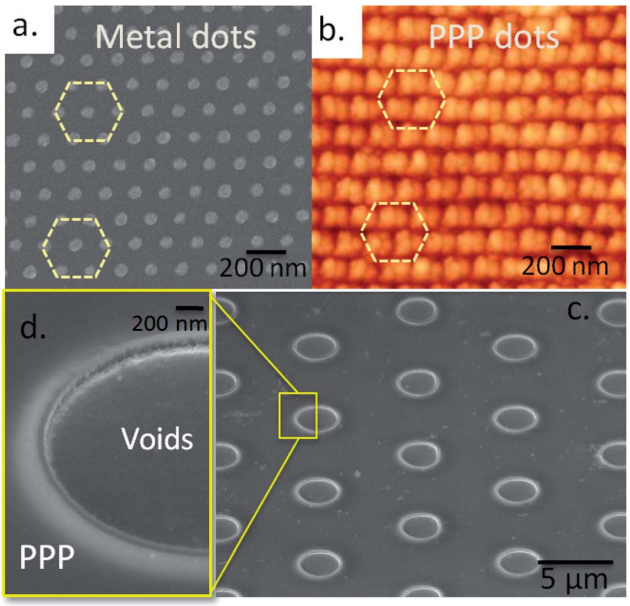

Fig. 4 Micro- and nano-pattern of PPP brush (M_n = 4k) created using the scheme in Fig. S4.† E-beam-lithography patterned Ni or Cr nanodots (a) are used to fabricate the starting metal nanopattern for PCHD precursor brush, which eventually leads to a well-defined PPP brush nanopattern (b). A large area micropattern of PPP brush (M_n = 4k) is shown in (c), and a close-up SEM image is given in (d).

modifications that lead to novel conjugated polymer systems have also been reported.[37–42] For example, Frechet, *et al.*, synthesized low band-gap benzothiadiazole and pyrrole based conjugated copolymers with thermally cleavable solubilizing groups as precursors so that their solubility and optoelectronic properties dramatically change upon thermal treatments,[41] while Bouffard *et al.* demonstrated that polymers made from 1,4-dialkoxy-1,4-diarylcyclohexane monomers could be converted to the conjugated poly(arylene dienylene) during photopatterning.[42] Although the post-polymerization chemistry used in this work pertains to aromatization of PCHD brushes, the notion of using chemical transformations after processing and patterning is a general strategy that is growing in practice and attractive for other conjugated polymer systems.[37–42]

In conclusion, we report optoelectronic properties, grafting density effects, and nanopatterning of well-defined conjugated poly(*para*-phenylene) brushes of various molecular weights that are made by chemical conversion of poly(cyclohexadiene)s having low polydispersities (PDI < 1.1). The use of this "precursor brush" route allows the grafting density of the PPP brush to be systematically varied, which seems to impact the effective conjugation length due to trade-offs between packing of chains and intrachain defects brought about by lateral crowding of the chains. The precursor brush approach also allows us to implement methods to micro- and nano-pattern conjugated polymer brushes. Together this work represents a path to elucidate how chain properties and confinement affects the optoelectronic properties of conjugated polymer brushes, a theme that is likely to be of practical importance for device systems.

Acknowledgements

Initial aspects of this work focused on synthesis and layer assembly were supported through the DOE Laboratory Directed Research and Development award program. A portion of the research was conducted at the Center for Nanophase Materials Sciences, which is sponsored at Oak Ridge National Laboratory by the Scientific User Facilities Division, Office of Basic Energy Sciences, U.S. Department of Energy (DOE). D.L. acknowledges partial support from NSF (award #ECCS-1151140). SMK and JWM acknowledge support from the U.S. Army Research Office through Grant no. W911NF-11-1-0417.

References

1 S. T. Milner, *Science*, 1991, **251**, 905–914.
2 B. Zhao and W. J. Brittain, *Prog. Polym. Sci.*, 2000, **25**, 677–710.
3 H. Sirringhaus, T. Kawase, R. H. Friend, T. Shimoda, M. Inbasekaran, W. Wu and E. P. Woo, *Science*, 2000, **290**, 2123–2126.
4 C. G. Wu and T. Bein, *Science*, 1994, **264**, 1757–1759.
5 N. Tessler, V. Medvedev, M. Kazes, S. H. Kan and U. Banin, *Science*, 2002, **295**, 1506–1508.
6 X. Gong, M. H. Tong, Y. J. Xia, W. Z. Cai, J. S. Moon, Y. Cao, G. Yu, C. L. Shieh, B. Nilsson and A. J. Heeger, *Science*, 2009, **325**, 1665–1667.
7 (*a*) V. Senkovskyy, N. Khanduyeva, H. Komber, U. Oertel, M. Stamm, D. Kuckling and A. Kiriy, *J. Am. Chem. Soc.*, 2007, **129**, 6626–6632; (*b*) S. K. Sontag, N. Marshall and J. Locklin, *Chem. Commun.*, 2009, **23**, 3354–3356.
8 (*a*) N. Marshall, S. K. Sontag and J. Locklin, *Chem. Commun.*, 2011, **47**, 5681–5689; (*b*) N. Marshall, S. K. Sontag and J. Locklin, *Macromolecules*, 2010, **43**, 2137–2144.
9 (*a*) N. Doubina, J. L. Jenkins, S. A. Paniagua, K. A. Mazzio, G. A. MacDonald, A. K. Y. Jen, N. R. Armstrong, S. R. Marder and C. K. Luscombe, *Langmuir*, 2012, **28**, 1900–1908; (*b*) L. Yang, S. K. Sontag, T. W. LaJoie, W. Li, N. E. Huddleston, J. Locklin and W. You, *ACS Appl. Mater. Interfaces*, 2012, **4**, 5069–5073.
10 (*a*) P. Paoprasert, J. W. Spalenka, D. L. Peterson, R. E. Ruther, R. J. Hamers, P. G. Evans and P. Gopalan, *J. Mater. Chem.*, 2010, **20**, 2651–2658; (*b*) D. Meng, J. Sun, S. Jiang, Y. Zeng, Y. Li, S. Yan, J. Geng and Y. Huang, *J. Mater. Chem.*, 2012, **22**, 21583–21591.
11 M. Banerjee, R. Shukla and R. Rathore, *J. Am. Chem. Soc.*, 2009, **131**, 1780–1786.
12 L. W. Shacklette, R. R. Chance, D. M. Ivory, G. G. Miller and R. H. Baughman, *Synth. Met.*, 1980, **1**, 307–320.
13 A. J. Berresheim, M. Muller and K. Mullen, *Chem. Rev.*, 1999, **99**, 1747–1785.
14 I. Natori, S. Natori, H. Sekikawa and H. Sato, *J. Polym. Sci., Part A: Polym. Chem.*, 2008, **46**, 5223–5231.
15 W. J. Song, C. Seoul, G. W. Kang and C. Lee, *Synth. Met.*, 2000, **114**, 355–359.
16 C. Seoul, W. J. Song, G. W. Kang and C. H. Lee, *Synth. Met.*, 2002, **130**, 9–16.

17 M. Remmers, B. Muller, K. Martin, H. J. Rader and W. Kohler, *Macromolecules*, 1999, **32**, 1073–1079.
18 J. Alonzo, J. Chen, J. Messman, X. Yu, K. Hong, S. Deng, O. Swader, M. Dadmun, J. F. Ankner, P. Britt, J. W. Mays, M. Malagoli, B. G. Sumpter, J.-L. Bredas and S. M. Kilbey, II, *Chem. Mater.*, 2011, **23**, 4367–4374.
19 J. Alonzo, W. M. Kochemba, D. L. Pickel, M. Ramanathan, Z. Sun, D. Li, J. Chen, B. G. Sumpter, W. T. Heller and S. M. Kilbey, II, *Nanoscale*, 2013, **5**, 9357–9364.
20 The approximate length of a PCHD monomer was determined from a full geometry optimization of a PCHD oligomer (consisting of 12 monomers with 1,4 intrachain linkages) using the MM3 force field, which is described by N. L. Allinger, Y. H. Yuh and J.-H. Lii, *J. Am. Chem. Soc.*, 1989, **111**, 8551–8566.
21 J. Bredas, R. Chance and R. Silbey, *Phys. Rev. B: Condens. Matter Mater. Phys.*, 1982, **26**, 5843–5854.
22 M. Winokur, P. Wamsley, J. Moulton, P. Smith and A. Heeger, *Macromolecules*, 1991, **24**, 3812–3815.
23 C. Chiang, C. Fincher, Y. Park, A. Heeger, H. Shirakawa, E. Louis, S. Gau and A. Macdiarmid, *Phys. Rev. Lett.*, 1977, **39**, 1098–1101.
24 J. Yu and S. Holdcroft, *Chem. Mater.*, 2002, **14**, 3705–3714.
25 P. Kuivalainen, H. Stubb, H. Isotalo, P. Ylilahti and C. Holmstrom, *Phys. Rev. B: Condens. Matter Mater. Phys.*, 1985, **31**, 7900–7909.
26 T. Shiga, A. Okada and T. Kurauchi, *Macromolecules*, 1993, **26**, 6958–6963.
27 Z. T. Zhou, S. H. Hu and H. J. Liu, *Polym. Adv. Technol.*, 1996, **7**, 667–670.
28 P. Phumman, S. Niamlang and A. Sirivat, *Sensors*, 2009, **9**, 8031–8046.
29 S. Holdcroft, *Adv. Mater.*, 2001, **13**, 1753–1765.
30 M. Renak, G. Bazan and D. Roitman, *Adv. Mater.*, 1997, **9**, 392.
31 F. Di Benedetto, A. Camposeo, S. Pagliara, E. Mele, L. Persano, R. Stabile, R. Cingolani and D. Pisignano, *Nat. Nanotechnol.*, 2008, **3**, 614–619.
32 R. K. Smith, P. A. Lewis and P. S. Weiss, *Prog. Surf. Sci.*, 2004, **75**, 1–68.
33 K. S. Kim, Y. Zhao, H. Jang, S. Y. Lee, J. M. Kim, K. S. Kim, J.-H. Ahn, P. Kim, J.-Y. Choi and B. H. Hong, *Nature*, 2009, **457**, 706–710.
34 C. J. Galvin and J. Genzer, *Prog. Polym. Sci.*, 2012, **37**, 871–906.
35 S. Kazuki, M. Takeuchi, N. Fujita, M. Numata and S. Shinkai, *Chem. Soc. Rev.*, 2007, **36**, 415–435.
36 R. M. Arnold, N. E. Huddleston and J. Locklin, *J. Mater. Chem.*, 2012, **37**, 19357–19365.
37 F. C. Krebs and K. Norrman, *ACS Appl. Mater. Interfaces*, 2010, **2**, 877–887.
38 C. Xie and P. M. Lahti, *J. Polym. Sci., Part A: Polym. Chem*, 1999, **37**, 779–788.
39 B. Van Veller and T. W. Swager, *Chem. Commun.*, 2010, **46**, 5761–5763.
40 B. J. Camo, J. Duchateau, C. R. Ganivet, B. Ballesteros, J. Gilot, M. M. Wienk, W. D. Oosterbaan, L. Lutsen, T. J. Clejj, G. de la Torre, R. A. J. Janssen, D. Vanderzande and T. Torres, *Dalton Trans.*, 2011, **40**, 3979.
41 C. Edder, P. B. Armstrong, K. B. Prado and J. M. J. Frechet, *Chem. Commun.*, 2006, **18**, 1965–1967.
42 J. Bouffard, M. Watanabe, H. Takaba and K. Itami, *Macromolecules*, 2010, **43**, 1425–1429.

